16th Australasian Fluid Mechanics Conference
Crown Plaza, Gold Coast, Australia
2-7 December 2007

An Application of a Second Order Upwinding Scheme for an Implicit LES CFD Solver

P.D.M. Brady, M. Gaston and J. Reizes

Faculty of Engineering
University of Technology Sydney, New South Wales, 2007 AUSTRALIA

Abstract

The flow past a right square cylinder in a duct at a Reynolds number of 22 x 10^3 has been employed to validate the use of second order upwinding, instead of a subgrid model in a large-eddy simulation. In this extensively studied problem, all the numerical work has been based on a simplifying assumption that the square cylinder is infinite, which resulted in all previous workers using cyclic boundary conditions so as to reduce the required domain size. It is not clear how the size of the domain had been established and, therefore, whether it was sufficiently large to adequately represent the experimental flow in a duct.

The integral quantities of the drag and lift coefficient and the Strouhal number, converged towards the experimental values as the grid resolution is increased. However, the cyclic boundary condition assumption leads to a flow width that provides too small a region of uncorrelated flow. A model of the full duct case, identical to experimental domain, was used to contrast the cyclic domain results. Surprisingly the second order upwind model generates power spectra that appear to correctly capture the energy cascade down to the inertial and viscous ranges.

Introduction

Despite many years of experimental, theoretical and numerical effort from the date of the discovery of turbulent flow by Reynolds late in the 19th Century [15], there is no coherent theory of turbulence. Much of the understanding about turbulence was initially generated from delicate experimental investigations, first using hot wires [20], then with LDA and recently with PIV [4]. There is, therefore, a very large body of experimental data that can be tapped. The advent of extremely powerful computers has also led to the development and use of numerical methods to simulate and model turbulence.

However, there is a caveat to this large body of data in that the vast majority is restricted to relatively simple single-phase flow regimes. Other investigations of the time, and later, focussed on boundary layer development, Prandtl [14] and Schlichting [17] and single fluid bluff body investigations such as the work of von Kármán. Unfortunately, until very recently there has been relatively little research into near surface turbulence, particularly around surface piercing bodies, bluff or streamlined.

In an effort to overcome the limited knowledge base of free-surface flows, a computational fluid dynamics code is being developed that is specifically designed for turbulent free-surface flows. However, as an intermediate step in the development of a validated free-surface code it is necessary to prove that the model and methods perform adequately for known single fluid cases. For single fluid validation a square cylinder in cross flow at transition was chosen [7]. The flow is complex with a several distinct regions: a quasi-periodic wake region; a laminar free-stream component and a transition boundary layer between the wake and free-stream.

As a necessity for modelling the detailed vortical motions of free-surface flows a Large Eddy Simulation (LES) based flow solver was implemented. Our model was based on a Second Order Upwind (SOU) discretisation scheme with no specific subgrid model which contradicts Grinstein's argument [6] that a higher order scheme is necessary to capture the flow physics. Presented in this paper are results from our SOU scheme, which was implemented in a commercial CFD solver: CFD-ACE+ [1]. The SOU model was compared with the extensively studied test case of a right square cylinder in duct flow at a Reynolds number of $22x10^3$. This test case was based on the experimental work of Lyn and Rodi [8] and Lyn et al [9] and was used as base case for a LES modelling workshop [16] and numerous CFD researchers, for example [3, 11, 18]. As a simplification, to reduce the number of model cells required, the workshop described in [16] prescribed a shortened spanwise axis and introduced spanwise periodic boundary conditions to compensate. This appeared to be an assumption with little justification, save the cell count reduction, so an additional model was developed, which was equivalent to the full duct experimental case as a reference.

In order to analyse the signals derived from the CFD models a method of analysis based on the Hilbert transform was developed. The Hilbert transform allows the researcher, via the computation of the analytic function, to estimate the phase angles of a signal relative to itself. This in turn allows the researcher to accurately compute a number of quantities including phase averages and local frequency variations. A similar method [20] was published in 1979 however little seems to have been done with the transform until recently. Perrin *et al* [12] used a technique that filtered the input signal prior to the computation of local phase angles. These phase angles were then used, together with a lowpass filtered version of the original signal, to compute the phase averages. The second signal was not filtered prior to averaging as the results indicate that the filtering process may lead to inaccuracies by changing the power of the filtered signal.

Problem Definition

Geometry and Boundary Conditions

The problem considered was a right square cylinder placed perpendicular to the free stream duct flow, Figure 1. Two cases were considered: the reduced specified for the 2nd ERCOFTAC Workshop on Direct and Large-Eddy Simulation and a larger geometry based on the full experiment from the investigations of [8], Table 1 and Figure 1. These runs are subsequently referred to as LES2 and BG respectively. Both cases were investigated at a Reynolds number of approximately $22x10^3$ based on the free stream velocity and the cylinder diameter. Extensive reference data from both the numerical workshop [13] and experimental investigations [7, 8] are available for comparison.

Run	D (m)	x_1 (m)	x_2 (m)	y_1 (m)	z_1 (m)
LES2	0.04	0.296	0.632	0.628	0.16
BG	0.04	0.296	0.632	0.560	0.39

Table 1 – Principal Dimensions

For both simulations the boundary conditions for the cylinder were prescribed as no-slip walls. Because wall functions are known to struggle with regions of massive separation, no wall functions were used in this simulation. The outflow boundaries were defined as constant pressure outlets and the inflows as constant velocity inlets.

The inlet velocity applied perpendicular and across the y-z inlet plane was uniform with no allowance for fully developed flow. However, to avoid impulse starts, and the associated pressure waves, the inlet velocity was ramped from zero at t=0s to full

speed at t=2s using a half sine wave, Figure 2. No allowance was made for turbulent fluctuations of the inlet velocity.

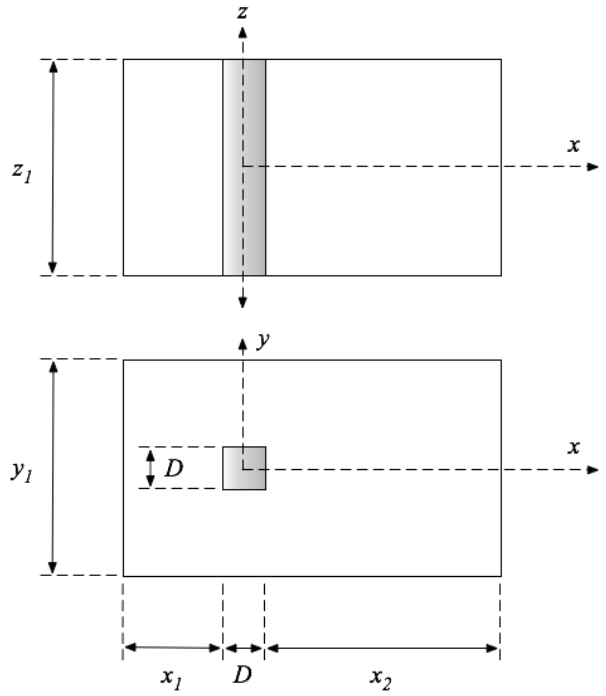

Figure 1 – Problem geometry and principal axes sketch

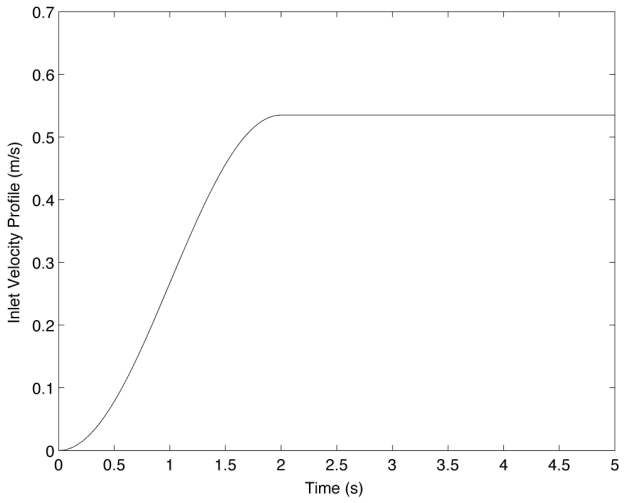

Figure 2 – Inlet velocity profile

For the LES2 case the span wise walls were defined as cyclic so that in theory the cylinder span would be infinite. The upper and lower boundaries were defined as non-slip boundaries that were implemented in the code as symmetry planes. For the BG case both the span wise and upper and lower boundaries were defined as walls, hence non-slip and no wall functions.

Numerical Methods

The research was carried out using the CFD-ACE+ package [1] developed by the ESI Group with the aim of applying a standard 2nd Order Upwind with Limiter solver to a novel situation. CFD-ACE+ is a general purpose, multi-physics capable finite volume CFD solver and utilises fully unstructured meshes and a parallel computation engine.

There are a number of potential limitations to this philosophy in that:

1. The researcher is limited by an external developer who maintains the code
2. Generally limited availability of source code documentation and numerical methodology

However, the main of advantage is that research time can be applied to a variety of problems rather than spent in the development of a code as a whole.

In this case the reader is referred to the CFD-ACE documentation that further refers the reader to [2] for a description of the Second Order Upwind with Limiter solver that was implemented with CFD-ACE+. However, the volume of data produced and the nature of the large scale periodic fluctuations meant a novel analysis technique was needed to interpret the data.

Hilbert Transform Based Analysis

The Hilbert transform, denoted as $h\{t\}$, is a convolution function that produces a signal, denoted as $\hat{s}(t)$, with a -π/2 phase shift relative to the original signal. This transformed signal is combined with the original signal such that

$$s_a(t) = s(t) + i \cdot \hat{s}(t) \quad (1)$$

where $s_a(t)$ is known as the analytic signal and i is the imaginary operator. From this analytic signal both the instantaneous amplitude (a) and phase angle (ϕ) can be derived. From these base parameters additional quantities such as the variation in frequency and relative phase angles may be derived.

Using the information contained in the Hilbert transform a number of additional parameters were computed. The first was to use a reference signal to accurately define phase angles for the calculation of phase averages and phase specific statistics. Secondly the instantaneous phase angle allows us to investigate the variance of frequency across the time domain, a quantity that is lost in a transform to the frequency domain.

The phase angle is directly calculated from the analytic signal

$$\phi = \arg\left(s_a(t)\right). \quad (2)$$

The amplitude of the instantaneous signal is computed as the absolute value of the analytic signal

$$a = \left|s_a(t)\right| = \sqrt{s(t)^2 + \hat{s}(t)^2}. \quad (3)$$

For example the calculated phase angle and amplitude of a continuous sine wave is a sawtooth phase angle curve and a constant amplitude line, Figure 3.

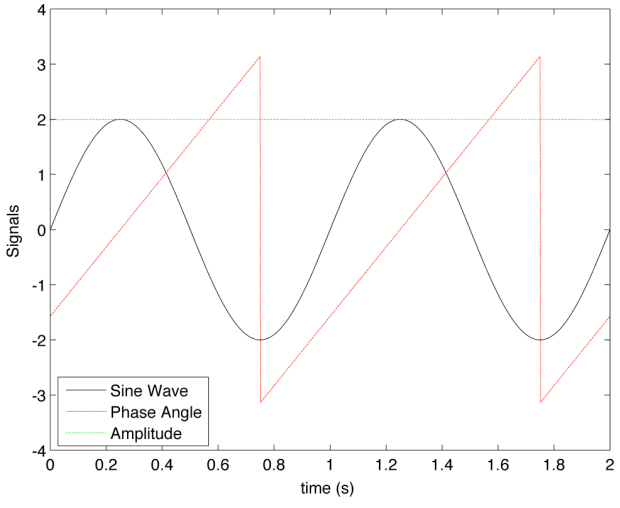

Figure 3 – Sine wave and Sample Output from a Hilbert transform

From the calculated phase angle it is possible to correlate a time domain coordinate with its location in the phase domain. This relationship forms the basis of the phase averaging method because, although the average is performed in the time domain, the data is filtered to include only points that fall within a defined phase domain envelope. Once the relative phase angle have been defined the standard decomposition for turbulent flow

$$u_i(t) = \overline{u}_i + u_i'(t), \quad (4)$$

where the three terms are the turbulent signal, the global average and the instantaneous fluctuations respectively, can be recast as

$$u_i(t) = \overline{u}_i + \overline{u}_{\phi i} + u_i'(t). \quad (5)$$

In this case the additional term in the decomposition is the average specific to a given phase angle. This decomposition better represents the information within regions of flow that experience significant periodic fluctuations such as within the wake region of bluff body flows. As this decomposition is more complex it is no longer valid to think of periodic flows as a single average but a collection of phase averages. Conversely this approach would neither be valid nor appropriate for uni-directional or isotropic turbulent flows.

If the individual phase averages are integrated across the respective phases, the statistics collapse to the traditional turbulent decomposition as the local phases average to zero. Therefore this method can be conceptualised as a super-set of the traditional decomposition method, which provides additional details on the periodic components.

Methods of signal analysis in the frequency domain typically rely on transforms such as the Fast Fourier Transform and Multi-Taper Methods. Although these algorithms provide estimates of the frequency based power density and confidence limits on that power density they both sacrifice locality in the time domain in terms of the frequency fluctuations. Use of the time derivative of the phase angle calculated from the Hilbert transform can overcome the time domain locality problem as the time derivative of a phase angle is a frequency. However, for real signals the derivative can generate a spiky signal for which it is generally acceptable to smooth the signal.

Mid Frequency Test Signal

The first test of the Hilbert method was a synthetic signal with a dominant frequency centred at 200Hz and sampled at 10kHz. Additional broadband noise at a signal to noise (SNR) ratio of 30:1 was added. This signal was chosen as the first test case because the dominant frequency was located away from the lower frequency boundary and it is, therefore, simpler to design a bandpass filter to isolate the dominant frequency.

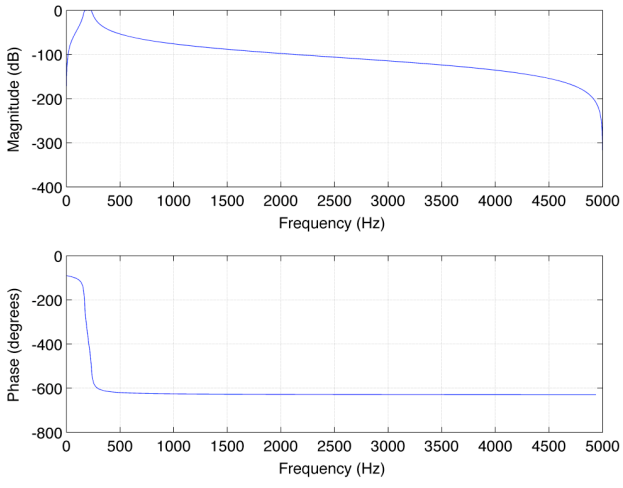

Figure 4 – Magnitude and Frequency response plot of the band pass filter

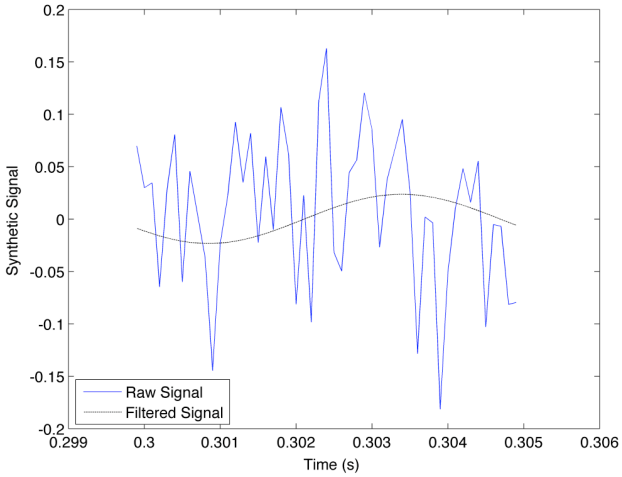

Figure 5 – Comparison of the Raw and Filtered Signals Relative to the Exact Sine Wave for the 200Hz Signal

In order to filter the noise components a third order Chebyshev Type I bandpass filter was designed with the lower and upper cut-off frequencies set to 170 and 230Hz respectively. The passband ripple was set to 0.5dB, Figure 4.

A non-causal filter was used such that there was no shift, or at least little, shift in the phase angle for the filtered signal relative to the input signal. A comparison of the filtered signal and the raw signal was performed to test the effect of the filter, Figure 5. It was observed that the filter effectively smoothed the spiky raw function to within ±0.6% of the ideal signal. For reference the variations imposed were in the range of ±6%.

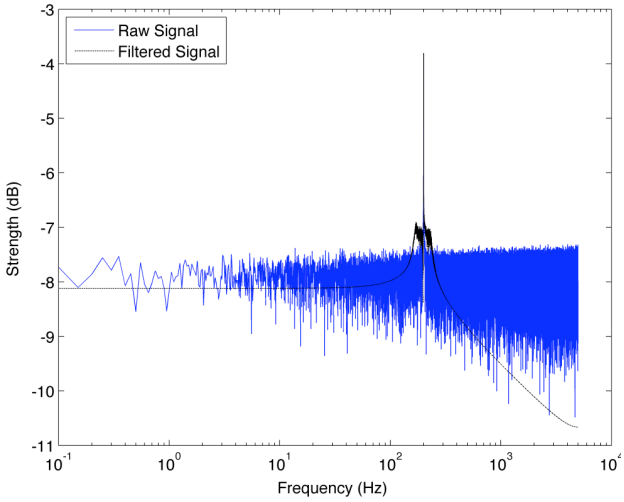

Figure 6 – Comparison of Positive Frequency FFT Coefficients for the Raw and Filtered 200Hz Signals

To provide a statistically significant data set the synthetic signal was arbitrarily chosen to be 20s long which equates to 4000 individual waves and 200×10^3 data points. This data set was then down converted into 16 individual phase sets that were 4000 points long. This number should be intuitive as there were 4000 waves so there should be 4000 data points in each of the individual phase sets but as the phase angle calculation and partitioning is done via an algorithm implemented in Matlab this is a vital validation parameter.

The phase averages were then computed for each of the 16 phase angles and the resultant averages compared with the exact signal, Figure 7. At this point, as with frequency domain analysis, all temporal locality data has been lost in favour of phase specific data. All phase averages were within $\pm 8 \times 10^{-15}$ of the exact

average, essentially machine precision, for that phase. When the average of the combined phases, or the global mean, was calculated the value was within a similar bound.

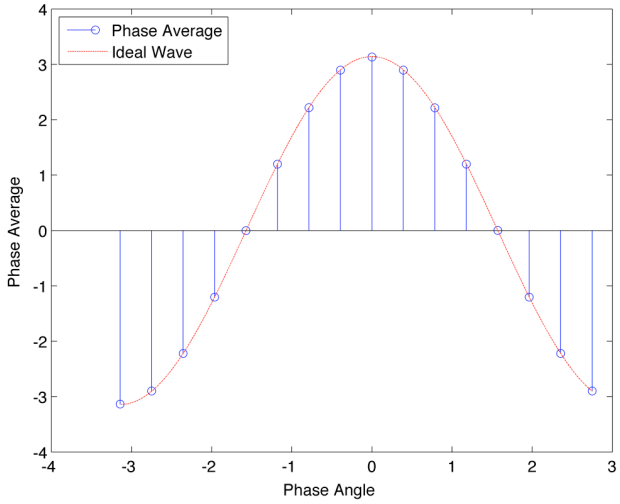

Figure 7 – Phase Average and Exact Average for the 200Hz Signal

In order to investigate the structure of the fluctuation from the phase averages, that is what we are interpreting as turbulence, the variation from the mean for an individual phase angle was plotted, Figure 8.

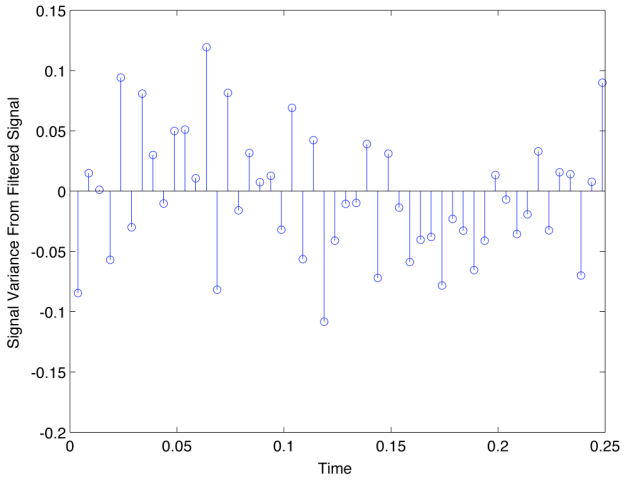

Figure 8 – Sample Set of Fluctuations from the Phase=-π Phase Average

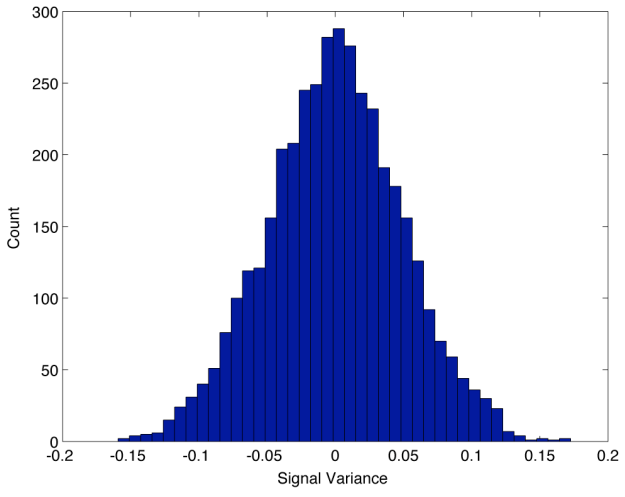

Figure 9 – PDF of Variance from the Phase=-π Phase Average

Although the data in Figure 8 has recovered both a fluctuation and it's associated location in the time domain, the plot by and of itself is of little value. A probability density function (PDF) of the fluctuations, Figure 9, is more interesting to describe the global properties of the fluctuation series.

The mean was calculated to be zero (to machine precision), variance of 0.005 and skew and kurtosis of approximately zero, Figure 9, which describe a PDF that is normally distributed. The results for the other 15 phases, not shown, are of the same order. This indicates that the method is able to successfully capture the global properties of the white noise that was superimposed on the base signal.

Low Frequency Test Signal

In order to test the analysis method on data that was closer to our real signal, a synthetic signal with a dominant frequency of 2Hz, with white noise at a SNR of 30:1 and sampled at 1kHz was generated. To generate a data set of equivalent statistical significance as the mid-frequency test this signal was extended in the time domain to 2000s.

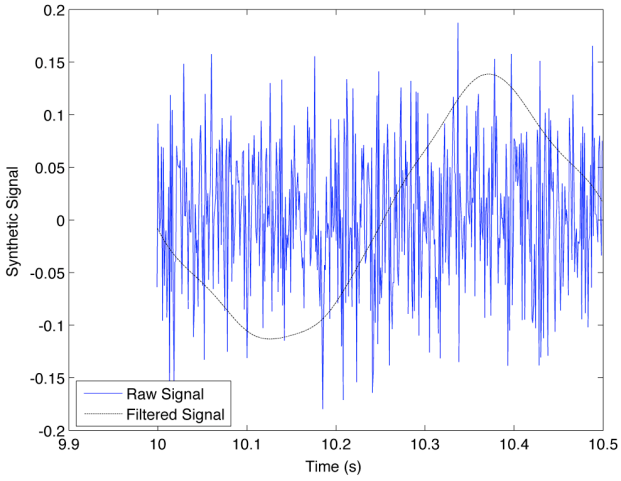

Figure 10 – Magnitude and Frequency response plot of the low pass filter

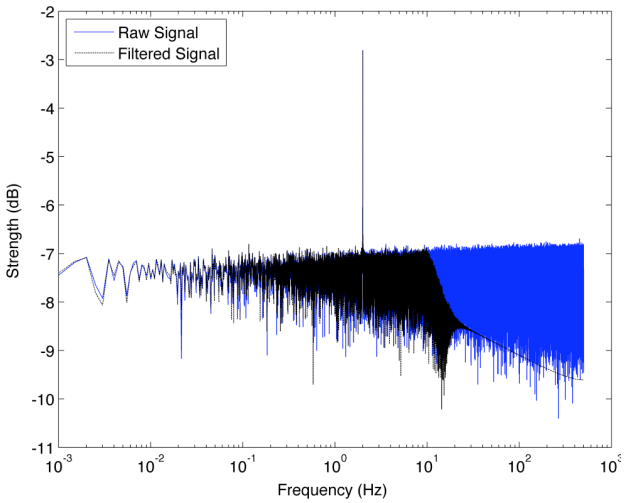

Figure 11 – Comparison of the Raw and Filtered Signal to the Exact Sine Wave for the 2Hz Signal

The method used to compute the fluctuations was the same as the Mid Frequency Test but in this case it was extremely difficult to design a bandpass filter for such a low passband. Therefore a low pass Chebyshev Type 1 filter with 0.5dB ripple and 10Hz cut off was designed, Figure 10. The use of a lowpass filter generated some additional fluctuations in the nominally clean

signal used to compute the phase angles. However low power fluctuations of the order of 1Hz on a 2Hz dominant signal are unlikely to have a statistically significant effect given their much lower, 50%, occurrence rate.

The lowpass filter did not capture the exact wave, Figure 11, as compared to the bandpass filter implemented for the mid-frequency test, Figure 5, which is probably due to the inclusion of the additional low frequency components below 2Hz. The FFT components of the raw and filtered signal are plotted for comparison, Figure 12. Although the bandgap appears significantly larger in the lowpass case this is an artefact of the semi-log scale on which the frequency axis was plotted. In fact the band gap of 10Hz for the lowpass case is significantly smaller than the 60Hz bandgap implemented in the bandpass filter.

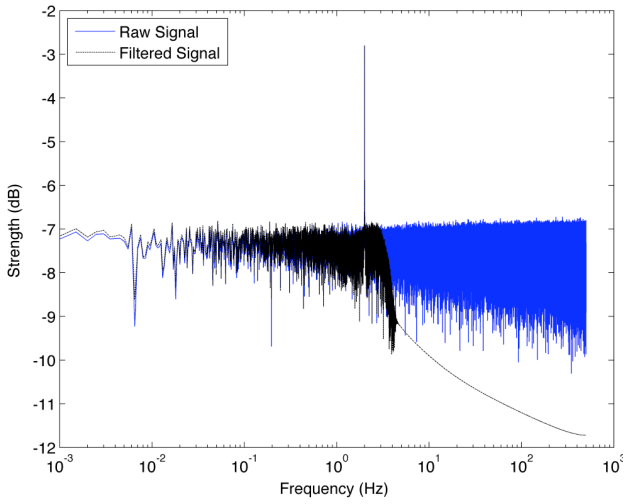

Figure 12 – Comparison of Positive Frequency FFT Coefficients for the Raw and Filtered 2Hz Signals

The sample reduction again successfully computed 4000 data points for each of the phase angles. The phase average fluctuations also tended to a zero mean normally distributed signal as would be expected from the superimposed white noise.

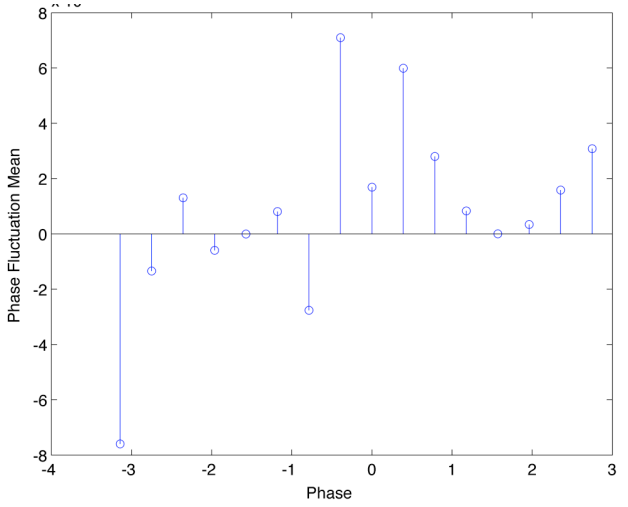

Figure 13 – Phase Angle Variances From the Phase Averages for the 2Hz Signal

With this sample set the variance from the phase averages across the phases was small, $\left|\sigma^2\right| < 7 \times 10^3$ and a visual inspection of the variance indicates no discernable pattern.

The conclusion from these synthetic tests is that the method of using

1. A filtered signal to provide a clean input for a
2. Hilbert transform to calculate phase angle locations to then use
3. The raw signal to calculate averages based on the computed phase locations

can successfully compute the fluctuations at individual phase angles. The caveat of this method is that you must be able to successfully isolate the global signal, in this case with a bandpass or lowpass filter, to be able to accurately compute the phase locations.

Model Validation

Table 2 shows the integral quantities calculated from the two model runs and comparison with other published results. To allow a suitable time for development of the flow field the first 10s of data were discarded from the calculations. The Strouhal number was calculated from the fluctuating lift signal using a FFT.

Run	Re ($x10^3$)	*Sr*	C_D	$C_{L'}$	$C_{D'}$	l_r	*Type*
LES2	22	0.124	2.47	1.51	0.37	0.71	C
BG	22	0.119	2.62	1.27	0.19	0.47	C
[18]	22	0.129-0.131	2.25 – 2.32	1.49 - 1.50	0.20 – 0.21	1.0 – 1.1	C
[16]	22	0.066 – 0.14	1.66 – 2.77	0.38 – 1.79	0.1 – 0.27	0.89 – 2.96	C
[19]	21.4	0.13 – 0.161	2.03 – 2.78	1.03 – 1.68	0.12 – 0.36	1.02 – 1.61	C
[9], [8]	21.4	0.13	2.1	-	-	1.38	E
[5]	22	-	2.0	0.5	-	-	E
[10]	23	-	-	1.3	-	-	E

Table 2 – Summary of Integral Quantities (Type C = CFD Results and Type E = Laboratory Results)

The Strouhal number calculated from the flow field is lower than the benchmark laboratory data ([8] and [9]) but well within the range of the published results. All other parameters fare similarly and are within the published range of experimental or numerical results.

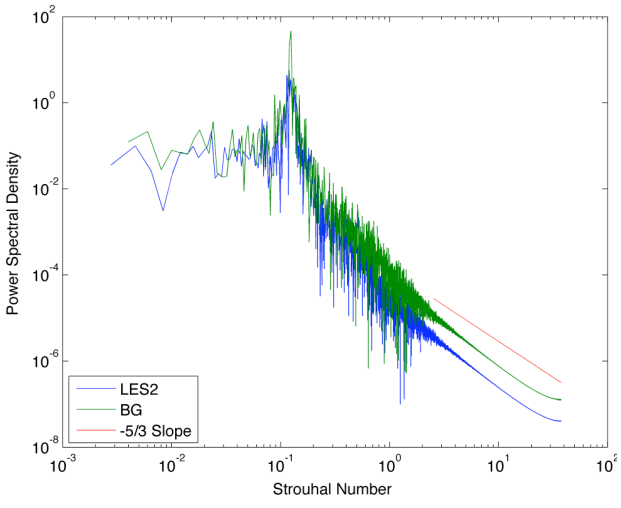

Figure 14 – Power spectral density of the fluctuating lift force

The slope of the PSD plot at the higher frequency ranges decays in proportion to $f^{5/3}$, which is a general indicator that the model is capturing the turbulent energy cascade, Figure 14. This result is particularly interesting given that there is no explicit turbulence model employed in the simulation.

The resultant drag coefficient for both models is towards the higher end of the published data. In addition the drag coefficient fluctuations are significantly higher for the LES2 model than the BG model. The variance of these results is probably due to several factors: the influence of the cyclic boundaries and the choice of time step. The region of flow within the cyclic boundaries appears too small to develop an adequate region of uncorrelated flow to sufficiently dominate the drag and lift integrals.

An additional potential for the variance is the different methods used to calculated the lift and drag. In the CFD case the pressure and shear forces were numerically integrated across the entire flow domain. However, as the published results do not indicate what method was used to calculate the forces, for example force balance in the wind tunnel or integrated from pressure taps, a thorough comparison is not possible.

The flow recovery length calculated from the time averaged flow field of our CFD model is smaller than the published results. This could indicate that there is too much dissipation generated within the model but further analysis of the model results is needed to establish this. However, despite the shorter recovery length the speed of the wake region recovers to approximately 70% of the free stream velocity and this recovery occurs within five cylinder lengths downstream of the cylinder, which is within the bounds of published results. Hence it is proposed that there cannot simply be too much dissipation, as the velocity should not recover to the 70% mark in an overly dissipative code.

The time step was arbitrarily chosen to be in the order of other comparison studies. Following the analysis presented here it is probable that the time step is too large and as such will cause additional unwanted dissipation in the internal computations.

Phase Averaged Results of the Fluctuating Lift

In order to apply the Hilbert phase method to the model data the first data set selected was the integrated lift force on the cylinder of the BG case. This data has a strong periodic component that is a result of the alternate vortex shedding from the sides of the cylinder. However, there is a potential problem with the choice of the lift signal as the integration process may remove some of the very irregularities that the method is designed to isolate.

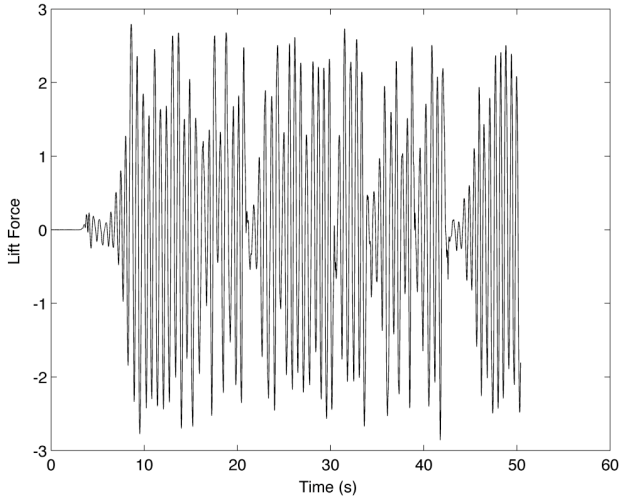

Figure 15 – Lift Integral Force on the Square Cylinder

The raw lift signal appears to exhibit a development phase from t=0s to approximately t=9s, Figure 15, which was removed from the analysis process.

Of itself the lift force is interesting in that it never truly repeats indicating that a steady state analysis is inappropriate. The fluctuations appear to be in the same order of magnitude but there also appears to be a regular pattern, for example at t=21s, 35s and 45s, where the lift dissipates for a short time period. Frequency domain analysis does not capture these discontinuities, Figure 14, and as such the signal may be more appropriate for wavelet analysis, which is more suited to frequency analysis of discontinuous signals.

The same 10Hz lowpass filter as designed for the Low Frequency test above was used to remove the high frequency components prior to calculation the Hilbert transform and the local phase angles, Figure 16.

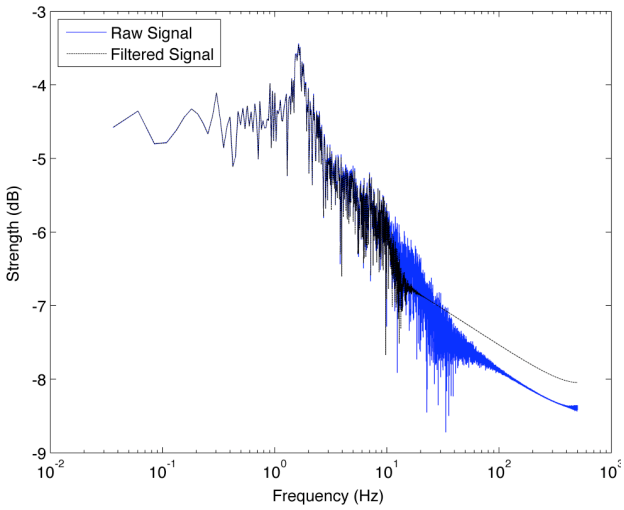

Figure 16 – Frequency Domain Representation of Real and Filtered Model Lift Data

The calculated phase angle data generated approximately 65 data points for the entire data set, or 65 unique waves. A rough calculation for a data set of 42s long shedding at around 1.8Hz would yield 75 individual waves for an ideal data set. Given the irregularities in the data our calculation of 65 waves is in the right order of magnitude. The phase averages were then calculated from the individual phase angle series, Figure 17.

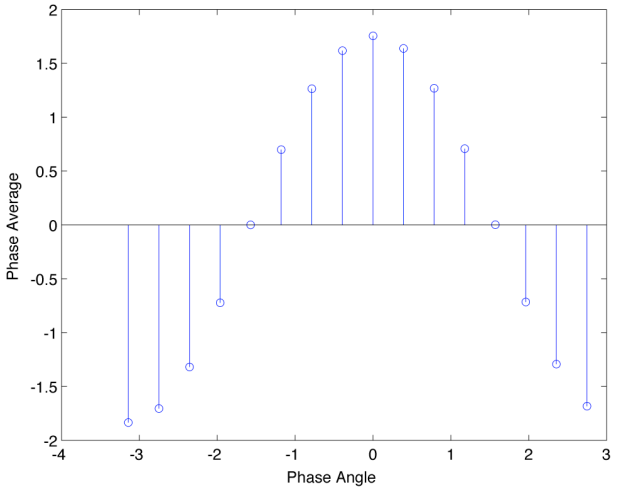

Figure 17 – Phase Averages for the Fluctuating Lift Signal

The phase averages exhibit the characteristic wave shape as expected, which is compared with the computed averages from

the ideal cases for example Figure 7. This is probably due to a much higher spread and uncertainty of the data in the real series and this is shown by the significantly higher variance, Figure 18.

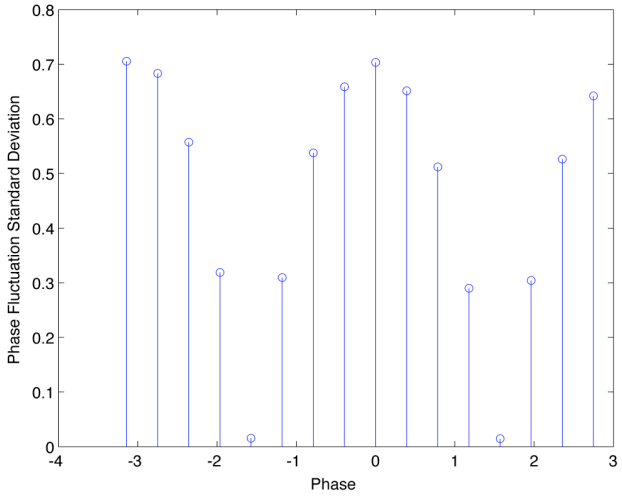

Figure 18 – Phase Angle Variance for the Fluctuating Lift Signal

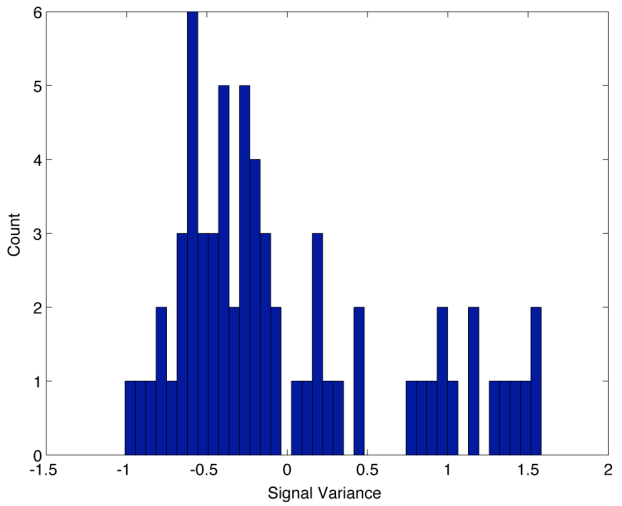

Figure 19 – PDF of the Phase=- π phase

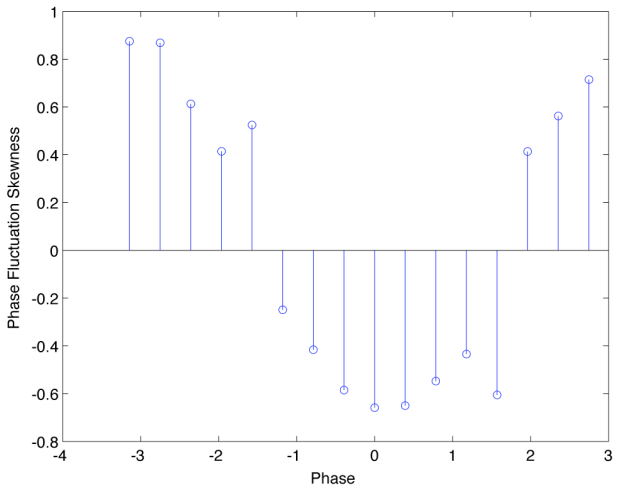

Figure 20 – Phase Angle Skewness for the Fluctuating Lift Signal

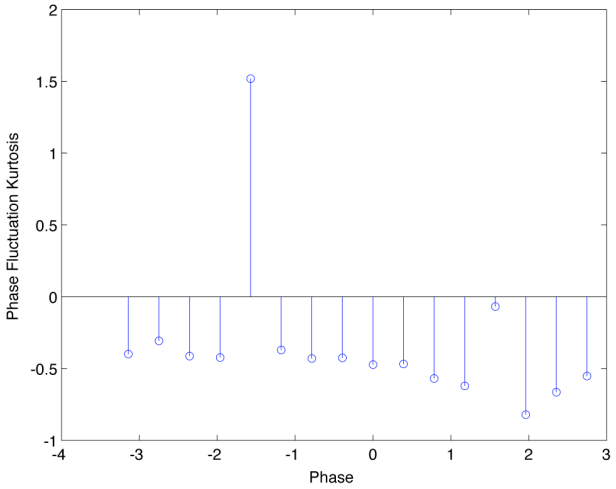

Figure 21 – Phase Angle Kurtosis for the Fluctuating Lift Signal

It is interesting to note that there appears to be a wave-like fluctuation in the variance plot, Figure 18. This wave-like behaviour is not apparent in the previous synthetic signals and at present there is no explanation for this phenomena – it may simply turn out to be a random pattern generated from the particular data set use. A statistical artefact with the human need to identify patterns.

Examination of the probability density function (phase=-π only plotted) and skew and kurtosis plots for all phase angles indicates that the data is not normally distributed: Figure 19, Figure 20 and Figure 21 respectively.

The apparently regular pattern observed in the signal variance has been carried forward into the skew. The kurtosis, save for a notable exception, appears to also exhibit a regular pattern, which is smaller in the size of the fluctuations than variance or skew. Again there is no theory as to the cause if this apparent regularity and further investigations are underway to isolate the causes.

Conclusions

A CFD based LES turbulence methodology has been developed and validated for a single fluid bluff body problem. Further an analysis technique was developed to investigate the fluctuations over the top of the periodic flow regime.

The validation of the model was justified on the basis of the comparison of a number of parameters including integral quantities, such as the lift and drag coefficients and their respective fluctuations. A frequency analysis was performed which showed that the power spectral density decayed in proportion to the -5/3 power law which is an accepted signature of turbulent flows.

The new analysis technique, based on a Hilbert transformation of a given data signals, was first validated on synthetic signals of known parameters. These synthetic signals were generated from single sine waves with an added white noise component and the analysis technique correctly recovered the statistical properties of both the underlying signal and the white noise components

References

[1] CFD-ACE+, V2006.0.33 ed. Huntsville, Alabama, USA: ESI Group, 2006.

[2] Barth, T. J. and Jespersen, D. C., The Design and Application of Upwind Schemes on Unstructured Meshes, in *27th Aerospace Science Meeting and Exhibition*. Reno, Nevada, USA: AIAA, 1989.

[3] Bouris, D. and Bergeles, G., 2D LES of Vortex Shedding from a Square Cylinder, *Journal of Wind Engineering and Industrial Aerodynamics*, vol. 80, pp. 31-46, 1999.

[4] Braza, M., Perrin, R., and Hoarau, Y., Turbulence Properties in the Cylinder Wake at High Reynolds Numbers, *Journal of Fluids and Structures*, vol. 22, pp. 757-771, 2006.

[5] Cheng, C. M., Lu, P. C., and Chen, R. H., Wind Loads on Square Cylinder in Homogenous Turbulent Flows, *Journal of Wind Engineering and Industrial Aerodynamics*, vol. 41, pp. 739-749, 1992.

[6] Grinstein, F. F., On Implicit LES for Turbulent Flows, presented in *Symposium on Modeling & Simulation of Variable Density & Compressible Turbulent Mixing*, Los Alamos National Laboratory, 2005.

[7] Lyn, D. A., Vortex Shedding Past Square Cylinder, vol. 2007, 1992.

[8] Lyn, D. A. and Rodi, W., The flapping shear layer formed by flow separation from the forward corner of a square cylinder, *Journal of fluid Mechanics*, vol. 267, pp. 253-376, 1994.

[9] Lyn, D. A., Einav, S., Rodi, W., and Park, J.-H., A laser-Doppler velocimetry study of ensemble-averaged characteristics of the turbulent near wake of a square cylinder, *Journal of Fluid Mechanics*, vol. 304, pp. 285-319, 1995.

[10] McLean, I. and Gartshore, I., Spanwise Correlations of Pressure on a Rigid Square Section Cylinder, *Journal of Wind Engineering and Industrial Aerodynamics*, vol. 41, pp. 797-808, 1992.

[11] Murakami, S. and Mochida, A., On turbulent Vortex Shedding flow Past 2D Square Cylinder Predicted by CFD, *Journal of Wind Engineering and Industrial Aerodynamics*, vol. 54/55, pp. 191-211, 1995.

[12] Perrin, R., Cid, E., Cazin, S., Sevrain, A., Braza, M., Moradei, F., and Harran, G., Phase-averaged measurements of the turbulence properties in the near wake of a circular cylinder at high Reynolds number by 2C-PIV and 3C-PIV, *Experiments in Fluids*, vol. 42, pp. 93-109, 2007.

[13] Pourquie, M. and Voke, P. R., Test Case LES2, vol. 2007, 1998.

[14] Prandtl, L., Über die ausgebildete Turbulenz, *ZAMM*, vol. 5, pp. 136-139, 1925.

[15] Reynolds, O., On the Dynamical Theory of Incompressible Viscous Fluids and the Determination of the Criterion, *Philosophical Transactions of the Royal Society of London, Series A*, vol. 186, pp. 123-164, 1895.

[16] Rodi, W., Ferziger, J., Breuer, M., and Pourquié, M., Status of Large Eddy Simulation: Results of a Workshop, *Journal of Fluids Engineering*, vol. 119, pp. 248-262, 1997.

[17] Schlichting, H., *Boundary Layer Theory*, 7th ed. New York: McGraw Hill, 1979.

[18] Sohankar, A., Davidson, L., and Norberg, C., A Dynamic One-Equation Subgrid Model for Simulation of Flow Around a Square Cylinder, presented in *4th International Symposium on Engineering Turbulence Modelling and Measurements*, Ajaccio, Corsica, France, 1999.

[19] Voke, P. R., Flow Past A Square Cylinder: Test Case LES2, presented in *Direct and Large Eddy Simulation II*, Grenoble, France, 1997.

[20] Wlezien, R. W. and Way, J. L., Techniques for the Experimental Investigation of the Near Wake of a Circular Cylinder, *AIAA Journal*, vol. 17, pp. 563-570, 1979.